NASA/TM-20240008991 GT2024–122380

Optimal Control Allocation for Distributed Electric Propulsion in a Series/Parallel Partial Hybrid Powertrain

Jonathan S. Litt
Glenn Research Center, Cleveland, Ohio

September 2024

NASA STI Program Report Series

Since its founding, NASA has been dedicated to the advancement of aeronautics and space science. The NASA scientific and technical information (STI) program plays a key part in helping NASA maintain this important role.

The NASA STI program operates under the auspices of the Agency Chief Information Officer. It collects, organizes, provides for archiving, and disseminates NASA's STI. The NASA STI program provides access to the NTRS Registered and its public interface, the NASA Technical Reports Server, thus providing one of the largest collections of aeronautical and space science STI in the world. Results are published in both non-NASA channels and by NASA in the NASA STI Report Series, which includes the following report types:

- TECHNICAL PUBLICATION.
  Reports of completed research or a major significant phase of research that present the results of NASA programs and include extensive data or theoretical analysis. Includes compilations of significant scientific and technical data and information deemed to be of continuing reference value. NASA counterpart of peer-reviewed formal professional papers but has less stringent limitations on manuscript length and extent of graphic presentations.

- TECHNICAL MEMORANDUM.
  Scientific and technical findings that are preliminary or of specialized interest, e.g., quick release reports, working papers, and bibliographies that contain minimal annotation. Does not contain extensive analysis.

- CONTRACTOR REPORT.
  Scientific and technical findings by NASA-sponsored contractors and grantees.

- CONFERENCE PUBLICATION.
  Collected papers from scientific and technical conferences, symposia, seminars, or other meetings sponsored or cosponsored by NASA.

- SPECIAL PUBLICATION.
  Scientific, technical, or historical information from NASA programs, projects, and missions, often concerned with subjects having substantial public interest.

- TECHNICAL TRANSLATION.
  English-language translations of foreign scientific and technical material pertinent to NASA's mission.

Specialized services also include organizing and publishing research results, distributing specialized research announcements and feeds, providing information desk and personal search support, and enabling data exchange services.

For more information about the NASA STI program, see the following:

- Access the NASA STI program home page at http://www.sti.nasa.gov

NASA/TM-20240008991 GT2024–122380

Optimal Control Allocation for Distributed Electric Propulsion in a Series/Parallel Partial Hybrid Powertrain

Jonathan S. Litt
Glenn Research Center, Cleveland, Ohio

Prepared for the
Turbo Expo 2024
sponsored by the the American Society of Mechanical Engineers (ASME)
London, England, United Kingdom, June 24–28, 2024

National Aeronautics and
Space Administration

Glenn Research Center
Cleveland, Ohio 44135

September 2024

Acknowledgments

This work was funded by the Transformative Aeronautics Concepts Program (TACP)/Convergent Aeronautics Solutions Project of the NASA Aeronautics Research Mission Directorate. The author thanks the SUSAN team for informative discussions on a variety of aspects related to the design and on aircraft operation in general. The author especially thanks Jonah Sachs-Wetstone and Jeff Chapman of NASA Glenn Research Center and Andrew Patterson of NASA Langley Research Center for providing model data and associated explanations.

This work was sponsored by the
Transformative Aeronautics Concepts Program.

Level of Review: This material has been technically reviewed by technical management.

This report is available in electronic form at https://www.sti.nasa.gov/ and https://ntrs.nasa.gov/

NASA STI Program/Mail Stop 050
NASA Langley Research Center
Hampton, VA 23681-2199

Optimal Control Allocation for Distributed Electric Propulsion in a Series/Parallel Partial Hybrid Powertrain

Jonathan S. Litt
National Aeronautics and Space Administration
Glenn Research Center
Cleveland, Ohio 44135

Abstract

The SUbsonic Single Aft eNgine (SUSAN) Electrofan is a NASA concept transport aircraft representative of technology anticipated for a 2040 entry-into-service date. The powertrain consists of a single thrust-producing geared turbofan engine with generators driving a series/parallel partial hybrid power/ propulsion system. The architecture includes 16 underwing contrarotating fans, eight on each side. The distributed fans can be used by the flight control system to augment or replace the rudder function. This paper sets up the optimal control problem of setpoint determination for individual wingfans in the distributed propulsion system, accounting for electrical string efficiencies, saturations, and failures. The solution minimizes power consumption while maintaining thrust and torque on the airframe for maneuvering. Additionally, thrust that would have been lost due to temporary fan speed or power saturation is optimally redistributed to maintain overall desired thrust and torque on the aircraft. A simulation of a coordinated turn utilizing the distributed electric propulsion for yaw rate control in a multiple wingfan failure scenario demonstrates the robustness of the powertrain design to failures and helps define its limitations.

Nomenclature

η_i	efficiency of the ith string
H	diag(η_1, …, η_n)
λ	Lagrange multiplier
ρ	air density
A	$[[1 \ldots 1]^T [r_1 \ldots r_n]^T]^T$
A_e	area of the engine face
a_i, c_i	coefficients
b	$[Fn\ Q]^T$
D	drag
fn_i	net thrust of the ith wingfan
Fn	Σfn_i, total net thrust
G	control reallocation gain matrix
g_i	ith column of G
I^*	Identity matrix with one or more of the columns removed
I_i	ith column of the identity matrix, I
J	objective function
n	number of wingfans
n_i	rotational speed of the ith wingfan
p_i	power consumed by ith wingfan motor (wingfan motor torque × wingfan motor rotational speed)
P	$[p_1, \ldots, p_n]^T$
P_{Tot}	Total power extracted to operate the wingfans
q	dynamic pressure
q_i	$r_i \times fn_i$, torque on aircraft due to ith wingfan
Q	$\Sigma(r_i \times fn_i)$, net torque on aircraft due to wingfans
r_i	distance of ith wingfan from centerline (i = 1 through n/2: positive; i = n/2+1 through n: negative)
u	vector of unmet thrust demands
v	aircraft speed relative to the air mass
w	vector of incremental thrust commands
x	independent variable, $[fn_1, \ldots, fn_n]^T$

1.0 Introduction

The SUbsonic Single Aft eNgine (SUSAN) Electrofan concept aircraft (Figure 1) is envisioned as the type of hybrid, single-aisle commercial jet that could enter into service in 2040. It utilizes electrified aircraft propulsion (EAP) technology to enable propulsive and aerodynamic benefits to reduce fuel usage and emissions. Although the design is still evolving, the current configuration (Ref. 1) has a single thrust producing, boundary layer-ingesting (BLI) geared turbofan (GTF) engine with generators driving a series/parallel partial hybrid EAP system. The architecture includes 16 underwing contrarotating BLI fans, or wingfans, eight on each side, in a mailslot configuration. The 16 fans run on power extracted from the GTF through four 5 MW generators connected to the Low-Pressure Spool (LPS), and a single 1 MW generator on the High-Pressure Spool (HPS). The wingfans generally provide about 65 percent of the thrust across the flight envelope while the GTF provides the remainder. The SUSAN concept includes single-use batteries for emergency wingfan power in case of GTF or generator failure.

The GTF is expected to be sized for cruise, meaning it is insufficient for some portion of takeoff and climb. To mitigate this, rechargeable batteries augment the extracted engine power during the most demanding phases of flight to

Figure 1.—Rendering of the current version of the SUSAN concept aircraft.

enable the wingfans to produce additional thrust. This power augmentation is known as boost. The batteries are subsequently recharged after the boost phase is complete through a small amount of additional power extraction from the GTF (Ref. 2).

To prevent thrust asymmetry in the case of a generator failure, the connections are interleaved such that each generator drives four wingfans selected to avoid thrust imbalance (Figure 2). The smaller HPS generator helps drive four wingfans, one from each set of four belonging the larger LPS generators. The constraints around powering the wingfans are related to power extraction from the GTF, power generation from the generator, and wingfan speed limitations.

The engine is designed for a given amount of power extraction at a given thrust setting, i.e., the engine thrust setting will determine the power extraction with only a small amount of variation allowed (Ref. 2) or the engine will move off its design point, reducing efficiency and operability. Each LPS generator can produce up to 5 MW, so the total power consumed by its four wingfans is limited to 5 MW, or 1.25 MW each. Each wingfan has a maximum rotational speed, which limits the power it can consume. Because of the boost capability, the wingfan rotational speed limit will not be reached during normal operation using extracted power alone.

The electrical portion of the powertrain is composed of strings, i.e., power flow paths, consisting of the components from the generator to the wingfan motor. The efficiency of the string is a function of the efficiencies of the individual components within it. Manufacturing variations will result in small differences between similar components, so the overall efficiency will vary from string to string. Thus, the amount of power required to be extracted from the GTF to drive a wingfan at a desired speed will depend on the efficiency of the string, i.e., the power required is p_i/η_i.

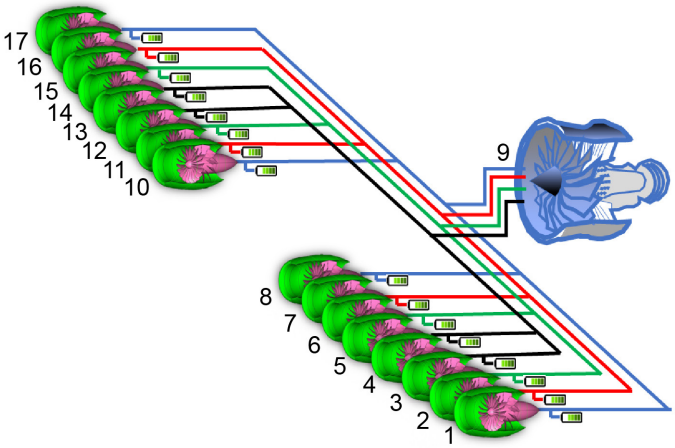

Figure 2.—SUSAN powertrain showing engine numbering, electrical bus coloring indicates which wingfans are connected to each LPS generator.

SUSAN leverages Distributed Electric Propulsion (DEP) for maneuvering. The flight control allows part or all of the rudder function to be assigned to the wingfans, which are evenly positioned at a distance from the aircraft's longitudinal axis (Figure 3). A thrust asymmetry produced using the wingfans differentially creates torque on the aircraft similar to the function of the rudder (Figure 4). Here, the power required for increased thrust on one side is balanced by reduced power corresponding to reduced thrust on the other side, approximately maintaining the total power draw. This provides the potential for reducing the rudder size and weight (Ref. 2). The incremental thrust commands from using DEP for turning are added to the nominal thrust commands based on throttle position (Figure 5).

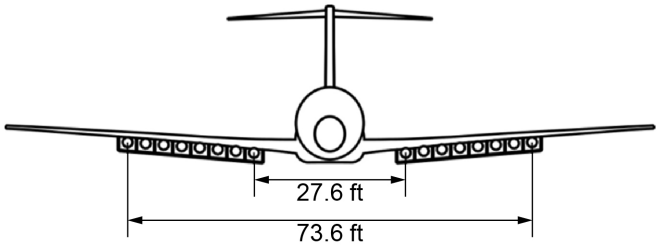

Figure 3.—SUSAN Front view showing wingfan locations. the measurements indicate that the wingfans are spaced about 3.3 ft on center.

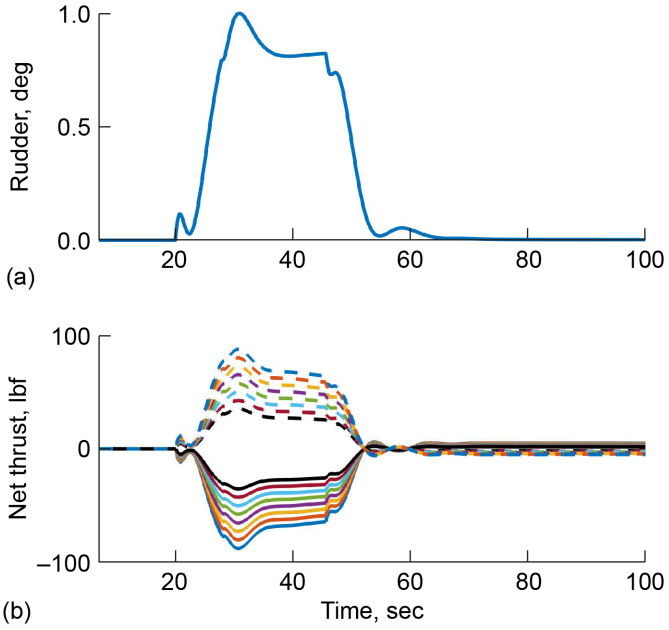

Figure 4.—Rudder movement during a coordinated turn at cruise (a). Equivalent incremental wingfan thrust commands for distributed electric propulsion (b). Solid lines are wingfans 1-8, dashed lines are 10-17. Outermost vary the most, innermost the least.

Fundamentally, this paper is about Integrated Flight/ Propulsion Control (IFPC), or the synergystic use of the flight control and propulsion subsystems to provide overall performance benefits (Ref. 3) and/or enhanced safety (Ref. 4). It builds on NASA's long history of promoting research on utilizing the engines for maneuvering (Ref. 5) and restructuring the control in response to failures (Ref. 6). New aircraft concepts with distributed propulsion lend themselves particularly well to these approaches, and the SUSAN design's built-in redundancy makes it a viable research platform for developing and evaluating relevant algorithms.

The current SUSAN configuration has been shown to close (Ref. 7), meaning that it meets the required objectives and constraints. However, there is still detailed design work going on, and some of the information used in this paper is based on

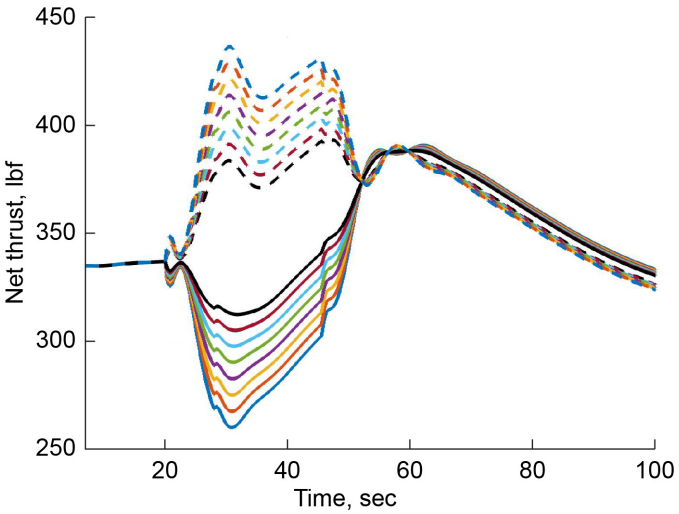

Figure 5.—Wingfan thrust during a coordinated turn at cruise including a temporary throttle increase.

studies performed for earlier iterations of the design, which introduces inconsistencies. This paper will point out the discrepancies and list the assumptions used for a proof-of-concept scheme for recovering the thrust lost when wingfan propulsors fail. The rest of this paper is organized as follows. The mathematical formulation for optimal control allocation that minimizes power consumption is presented next. This is followed by a description of the reallocation of thrust commands in the case of failures or saturations. Next, the problem as it applies to the SUSAN powertrain is laid out in terms of limits and constraints, followed by approximations and assumptions. With this context, an illustrative example is presented, followed by conclusions.

2.0 Optimal Control Allocation

The problem is to minimize power required while maintaining total net thrust and net torque on the airframe. Figure 6 shows the relationships between wingfan rotational speed, net thrust, and power (wingfan motor torque × wingfan motor rotational speed). Note that a gearbox reduces the wingfan rotational speed to 1/7.5 of that of the wingfan motor. For the initial derivation, Sea Level Static (SLS) is the selected operating condition because it has the ideal characteristics: there is a linear relationship between net thrust and speed, and a quadratic relationship between power and speed and thus between power and net thrust. Net thrust is the independent variable, from which the rotational speed setpoint can be directly calculated. The target (ideal) total thrust and net torque on the aircraft at any point in time are computed from the baseline wingfan thrust commands including the DEP increments (Figure 5). The optimization uses the method of Lagrange multipliers.

$$p_i = a_1 fn_i^2 + a_2 fn_i + a_3 \tag{1}$$

$$fn_i = c_1 n_i + c_2 \tag{2}$$

$$Ax = b \tag{3}$$

$$A = \begin{bmatrix} 1 & \cdots & 1 \\ r_1 & \cdots & r_n \end{bmatrix} \tag{4}$$

$$b = \begin{bmatrix} Fn \\ Q \end{bmatrix} \tag{5}$$

$$P = \begin{bmatrix} a_1 x_1^2 + a_2 x_1 + a_3 \\ \vdots \\ a_1 x_n^2 + a_2 x_n + a_3 \end{bmatrix} \tag{6}$$

$$\begin{aligned} P_{Tot} &= [1 \ldots 1] H^{-1} P \\ &= x^T a_1 H^{-1} x + [1 \ldots 1] a_2 H^{-1} x + a_3 tr(H^{-1}) \end{aligned} \tag{7}$$

$$J = \frac{1}{2} P_{Tot} + \lambda^T (b - Ax) \tag{8}$$

$$\frac{\partial J}{\partial x} = a_1 H^{-1} x + \frac{a_2}{2} H^{-1} [1 \ldots 1]^T - A^T \lambda = 0 \tag{9}$$

$$\frac{\partial J}{\partial \lambda} = b - Ax = 0 \tag{10}$$

$$x = \frac{1}{a_1} H A^T \lambda - \frac{a_2}{2a_1} [1 \ldots 1]^T \tag{11}$$

$$\lambda = a_1 (AHA^T)^{-1} b + \frac{a_2}{2} (AHA^T)^{-1} A [1 \ldots 1]^T \tag{12}$$

$$x = HA^T (AHA^T)^{-1} b + \frac{a_2}{2a_1} (HA^T - I)[1 \ldots 1]^T \tag{13}$$

This is the basic formulation. However, SLS is, by definition, not a flight condition, and Figure 7 shows that at cruise, there is a quadratic relationship between power and speed and between net thrust and speed, while there is a linear relationship between net thrust and power. The problem can be formulated as a function of speed, making both the objective function and constraint quadratic, but this is potentially a more difficult problem to solve than with a linear constraint, and may not have a closed form solution. Alternatively, setting up the problem as a function of net thrust gives a linear objective and a linear constraint. The basic optimal solution for a linear objective does not utilize all the inputs, i.e., it will utilize the minimum number of wingfans that meet the constraint and others will not be used (Ref. 8) or produce just enough thrust to offset their drag; because of the thrust available for boost, this is a realistic scenario. Clearly it is preferable to use all wingfans since otherwise they are merely excess weight. Therefore, in this case it makes sense to modify the objective from minimizing the total power consumed to minimizing the square of the power consumed. This provides a near optimal solution for power consumption while utilizing all wingfans. For convenience in the derivation of this quadratic formulation, we replace H^{-1} with $H^{-1/2}$.

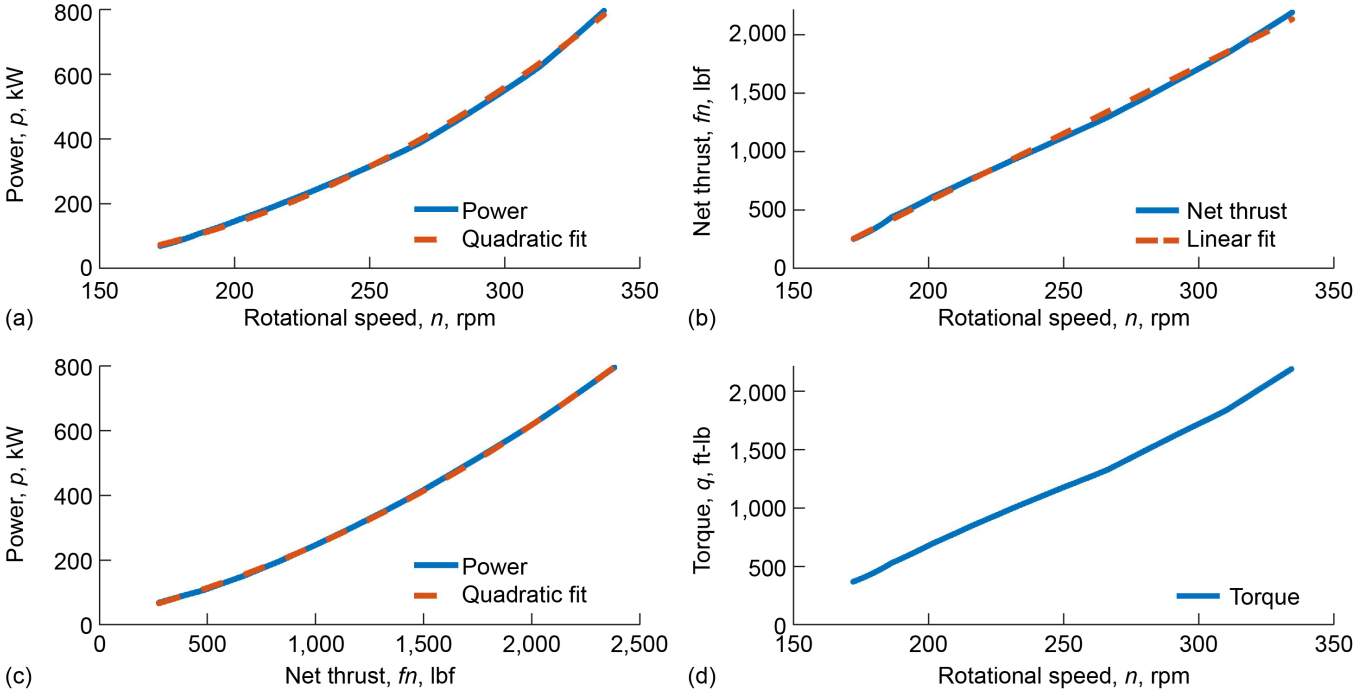

Figure 6.—Motor power, net thrust, and motor torque vs. fan rotational speed, and motor power vs net thrust at SLS. (a) Wingfan motor power vs. shaft speed. (b) Wingfan net thrust vs. shaft speed. (c) Wingfan motor power vs net thrust. (d) Wingfan motor torque vs. shaft speed.

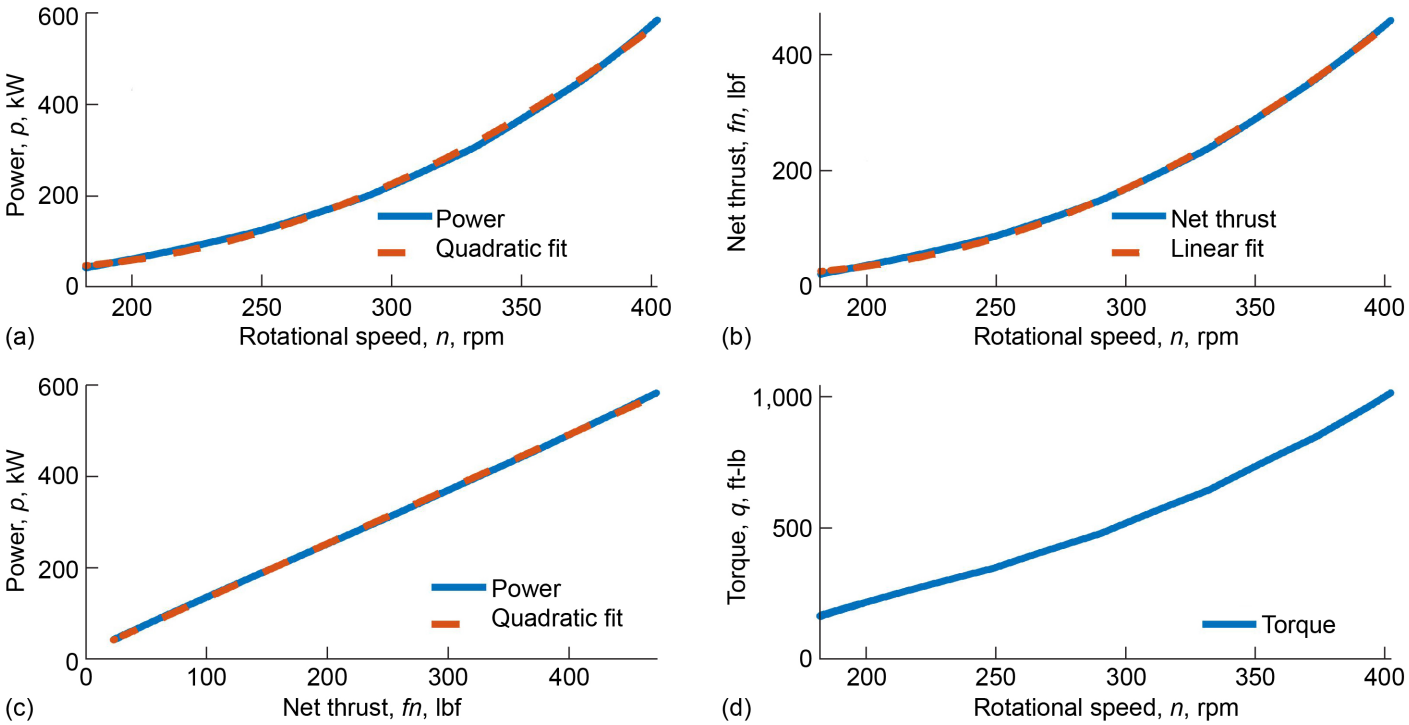

Figure 7.—Motor power, net thrust, and motor torque vs. fan rotational speed, and motor power vs net thrust at 35,000 ft, 0.785 MN. These are based on a design that does not account for boost. (a) Wingfan motor power vs. shaft speed. (b) Wingfan net thrust vs. shaft speed. (c) Wingfan motor power vs. net thrust. (d) Wingfan motor torque vs. shaft speed.

$$p_i = a_1 fn_i + a_2 \tag{14}$$

$$Ax = b \tag{15}$$

$$A = \begin{bmatrix} 1 & \cdots & 1 \\ r_1 & \cdots & r_n \end{bmatrix} \tag{16}$$

$$b = \begin{bmatrix} Fn \\ Q \end{bmatrix} \tag{17}$$

$$H^{-\frac{1}{2}}P = a_1 H^{-\frac{1}{2}}x + a_2 H^{-\frac{1}{2}}[1 \ldots 1]^T \tag{18}$$

$$\begin{aligned} J &= \frac{1}{2}\left(H^{-\frac{1}{2}}P\right)^T H^{-\frac{1}{2}}P + \lambda^T(b - Ax) \\ &= \frac{1}{2}\left(a_1^2 x^T H^{-1}x + 2a_1 a_2[1 \ldots 1]H^{-1}x + a_2^2 tr(H^{-1})\right) \\ &\quad + \lambda^T(b - Ax) \end{aligned} \tag{19}$$

$$\begin{aligned} \frac{\partial J}{\partial x} &= a_1^2 H^{-1}x + a_1 a_2 H^{-1}[1 \ldots 1]^T - A^T\lambda \\ &= 0 \end{aligned} \tag{20}$$

$$\frac{\partial J}{\partial \lambda} = b - Ax = 0 \tag{21}$$

$$x = \frac{1}{a_1^2} HA^T\lambda - \frac{a_2}{a_1}[1 \ldots 1]^T \tag{22}$$

$$\lambda = a_1^2(AHA^T)^{-1}b + a_1 a_2(AHA^T)^{-1}A[1 \ldots 1]^T \tag{23}$$

$$\begin{aligned} x = {} & HA^T(AHA^T)^{-1}b \\ & + \frac{a_2}{a_1}(HA^T(AHA^T)^{-1} - I)[1 \ldots 1]^T \end{aligned} \tag{24}$$

Interestingly, the solution for x (both Eqs. (13) and (24)) contains a constant term that does not depend on b. It clearly satisfies the constraint equation ($Ax = b$) as can be seen by pre-multiplying by A, causing those terms to cancel out, meaning that they do not impact the total thrust and net torque on the aircraft. However, their presence does reduce the power requirement.[1] Furthermore, adjusting the weighting matrix H to provide a greater penalty on the use of less efficient strings results in a noticeable power savings. In the above derivation

[1]The constant terms come from the curve fit, so the theoretical power savings they provide will only be realized if the model accurately represents the wingfans' thrust to power relationship.

we used $H^{-1/2}$ as the penalty, which reduces the differences in the weighting of the efficiencies, but simply replacing H by H^2 or H to an even higher power emphasizes the differences between the lower and higher efficiency strings, forcing more and more of the thrust output to the more efficient strings as the exponent is increased. While still utilizing all available wingfans, this approach drives the solution toward that of the linear programming approach (linear objective), which will use only the most efficient strings and not use the others at all.

To demonstrate, we assume that the efficiency of an individual string can be anywhere between 90 and 99 percent and that it is known with reasonable accuracy. Creating the weighting matrix H using such values on the diagonal produces a set of wingfan commands that is equivalent to those in Figure 5 in terms of total thrust and net torque on the aircraft, but with reduced power consumption. Figure 8 shows the same coordinated turn as in Figure 5 but with wingfan thrust setpoints optimized to minimize power consumption. Figure 8(b) and (c) show that total commanded wingfan thrust and net torque on the aircraft match those of the original, nonoptimized commands. In this case, the weighting matrix was H^8, as explained above, to enhance the separation between the most and least efficient strings. Figure 9 shows the power extracted by the LPS generators for three cases; the small HPS generator is ignored. Figure 9(a) shows the optimized case corresponding to Figure 8; here the most efficient strings are commanded to produce the most thrust and as a result consume the most power. Figure 9(b) shows the case corresponding to Figure 5, which does not account for efficiency; here the baseline wingfan commands are used, resulting in the least efficient strings consuming the most power. Compared to Figure 9(a), the vertical position of the power extraction curves is reversed. Figure 9(c) shows the power consumed in the ideal case where all strings are 100 percent efficient; in this case, all generators produce the same amount of power. The power initially consumed by the wingfans (at time 10 sec, for instance, before the turn begins) for the nonoptimized case (Figure 5) is about 7,067 kW, while in the optimized case (Figure 8) it is about 7,039 kW, a savings of about 0.4 percent for the specific randomly selected efficiency values. For comparison, the total power consumed in the ideal case is about 6,860 kW at the 10 sec mark.

Thus, we have solved the minimum power consumption problem in terms of thrust commands, but ultimately the solution must be in terms of fan speed commands. Figure 7(b) shows the quadratic relationship between net thrust and fan speed at the cruise condition. If the curve is represented as

$$fn_i = c_1 {n_i}^2 + c_2 n_i + c_3 \tag{25}$$

then the inverse function that gives fan rotational speed in terms of thrust is

$$n_i = \pm \sqrt{\frac{fn_i - c_3}{c_1} + \frac{{c_2}^2}{4{c_1}^2}} - \frac{c_2}{2c_1} \tag{26}$$

with the appropriate sign selected so that the range and domain are consistent with the *fn* vs. *n* curve in Figure 7(b). For the cruise case shown in Figure 7, the coefficients c_1 through c_3 are 0.0074, –2.3461, and 208.8562, respectively, with a domain of $n > 182$ rpm and range of $fn > 28$ lb. This curve fit gives an R^2 value of 0.9997.

In the power vs. *fn* plot in Figure 7(c), the coefficients a_1 and a_2, corresponding to Equation (14), are 1.2275 and 15.4742, respectively, which gives an R^2 value of 0.9998.

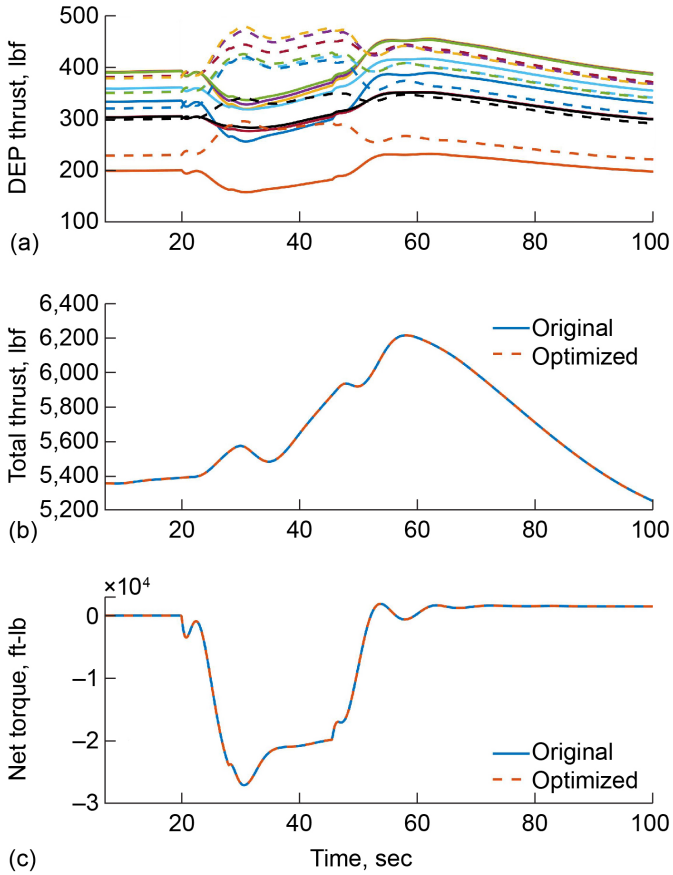

Figure 8.—(a) Optimized wingfan thrust setpoints, (b) total wingfan thrust for both original and optimized commands, and (c) net torque on aircraft for both original and optimized commands.

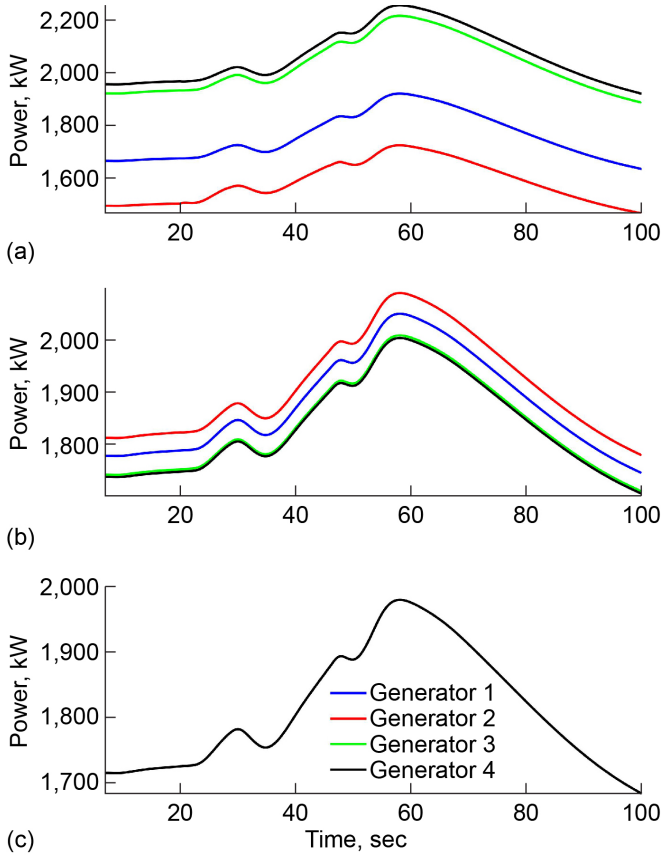

Figure 9.—(a) Power consumed during a coordinated turn for the optimized case corresponding to Figure 8, (b) nonoptimized case corresponding to Figure 5, and (c) ideal (100 percent efficient) case. The color corresponds to the bus color in Figure 2.

3.0 Wingfan Failures and Saturations

The SUSAN configuration with its 16 wingfans provides plenty of redundancy in case of failure. A wingfan failure might be the result of an electrical problem, i.e., a failure in one of the components in the string that powers it, or a mechanical problem such as a bearing failure or a bird strike. A main generator failure will cause its four wingfans to lose power. It should be noted that electrical components tend to operate in a consistent way until they fail fairly abruptly, meaning that their efficiency is generally constant over their life. Notable exceptions such as brushed motors are not considered for use in the SUSAN powertrain, and while future battery technology is anticipated to be incorporated, the work described in this paper specifically avoids the use of batteries. A saturation results from a speed setpoint command outside the range of operation of the fan, i.e., above the upper limit or below the lower limit, so the fan speed is unable to track the setpoint.

Whether caused by a saturation or failure, if any of the coordinated wingfans are unable to track their requested speed command, a throttle increase will be required to maintain total thrust, and the aircraft's flight control surfaces will be required to counteract the torque imbalance. Beyond that, the lost thrust equates to lost power extraction, which can move the engine away from its design point to a less efficient operating point or a region of unstable operation (Ref. 9). However, the redundancy enables redistribution of the lost thrust to maintain both total thrust and net torque within the limits of the system without loss of power extraction. The Windup Feedback algorithm (Refs. 10 and 11) was designed to redistribute unmet actuator demand to the remaining actuators in such a way that the system outputs maintain their ideal trajectories. This redistribution can result in additional saturations, and that unmet demand is then redistributed among the remaining unsaturated actuators up to the limits of the system. In this way, the supplemental actuator commands that result from saturations provide continuous commands to all non-failed actuators. The algorithm works by computing a gain matrix for the unmet demand corresponding to the remaining unsaturated actuators. With each subsequent saturation, the new unmet demand is distributed to the still-unsaturated actuators through a gain matrix designed for only those remaining actuators.

In the case of a failure or saturation, the lost thrust and resulting torque component are reconstructed through modifications to the remaining unsaturated wingfan commands. The unmet demand is passed through a 16×16 matrix, G, that distributes it to the remaining wingfans. With each new failure or saturation of, say, the ith wingfan, the ith column, g_i, of the matrix is computed as

$$g_i = I^* H A^T (A H I^* A^T)^{-1} A I_i \tag{27}$$

where I^* is the identity matrix with the dimension of the number of wingfans, 16 in this case, with the columns corresponding to the failed wingfans zeroed. Note that this description assumes the renumbering of the wingfans from 1 to 16, ignoring the GTF; it is understood here that columns 9 to 16 correspond to wingfans 10 to 17, respectively. I_i is the ith column of the identity matrix. Only the column corresponding to a new failure or saturation is computed, the existing columns are unchanged. H again is the diagonal matrix of the electrical string efficiencies, optimizing the redistribution of unmet thrust. The vector of incremental commands to the wingfans, w, is computed by multiplying the 16×1 vector of unmet demands, u, (with a value of 0 for each wingfan that can achieve its setpoint) by G.

$$w = Gu \tag{28}$$

In the case of saturation or failure, this incremental thrust command vector, w, is added to the original thrust command

vector, x, to create a new command vector that enables the system outputs (total thrust and net torque) to maintain their ideal trajectories up to the limits of the powertrain. Because the redistribution of unmet demand from a saturated wingfan can contribute to or even cause additional saturations, the newly computed columns of G have fewer nonzero elements over time, corresponding to the reduced number of unsaturated wingfans available for redistribution. Each time a wingfan saturates, the corresponding column of G is computed. Therefore, if a saturated wingfan unsaturates and then resaturates, the corresponding column of G is recomputed because a different combination of wingfans may be saturated at the later time. The computed columns of G correspond to the nonzero elements of u.

4.0 Limits and Constraints

Electronic components maintain performance regardless of altitude. Thus, the main generators' ability to produce power is not affected by flight condition. The performance of the air-breathing engine is strongly impacted by altitude, however, so the power available to be extracted changes with flight condition. The maximum power extraction, about 20 MW, occurs at takeoff, while at cruise that number is significantly less, about half in the current design. The design ensures that there is sufficient power available to maintain normal operation around the flight envelope. Any one LPS generator is limited to 5 MW of power extraction. Furthermore, based on the generator design, the power that can be extracted for any one wingfan is restricted to 1.25 MW and thus the power electronics are sized for this maximum load. This is sufficient for normal operation but can potentially become an active constraint for thrust reallocation due to failures and saturations at certain low-altitude, high-power conditions. The wingfans' normal range of operating speeds is well within the physical limits of the hardware. Recall that they are designed to support boost at top of climb (TOC), meaning that during the boost phase, the wingfans' thrust and thus rotational speed is significantly higher at cruise altitude than is actually necessary for cruise. The physical wingfan speed limit will depend on the design and the operating condition in terms of aeromechanical effects, efficiency penalties, etc.; here it is selected arbitrarily to be at the upper end of boost. It should be noted for completeness that the SUSAN wingfan concept (Ref. 12), which is a two-stage ducted fan (Figure 10), is designed to operate at rotational speeds in the thousands of rpm, as opposed to hundreds of rpm in this work to produce the same thrust.

The above observations will be leveraged to help accommodate wingfan failures, allowing the aircraft to continue flying without resorting to using emergency power (single use batteries to power the wingfans) up to the limits of the powertrain.

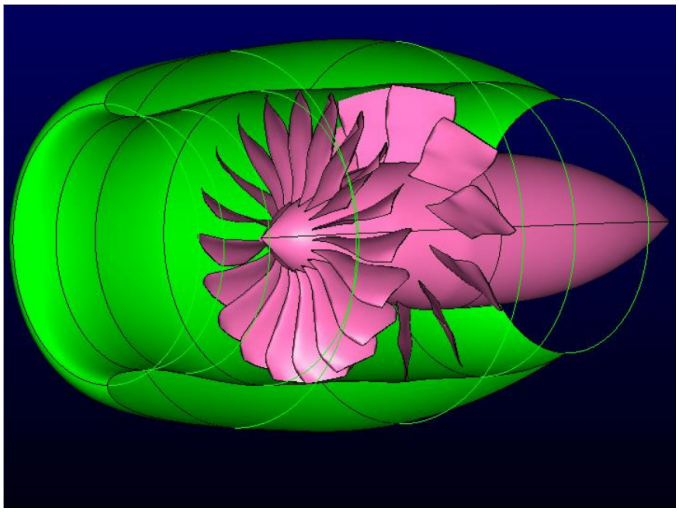

Figure 10.—Contrarotating electric fan.

5.0 Approximations and Assumptions

As the SUSAN design has evolved, trade studies (Ref. 13) optimized the individual subsystems for one configuration or another. Because findings from these various studies are used here, it has resulted in inconsistencies. Ultimately, these will have to be reconciled, but at this point, there are discrepancies that need to be worked around. In this section we develop assumptions that allow the representative analysis to proceed in a meaningful way.

When a wingfan fails, it not only loses thrust, but it also contributes additional drag. Thus, the remaining wingfans must counteract the drag in addition to replacing the lost thrust. Some analysis of the drag due to SUSAN's wingfans was performed, but not for the current configuration (Ref. 14). As mentioned above, the wingfans in this configuration are envisioned to be BLI, meaning that they accelerate the slower moving boundary layer air, providing an efficiency benefit. However, a detailed analysis (Ref. 15) determined that the fraction of low momentum flow across the total capture area is relatively small given the short distance the flow has to develop the boundary layer. Consequently, the average inlet Mach number across the wingfans is only slightly less than that of the freestream. For the purposes of this paper, wingfan drag at the cruise condition of 35,000 ft, Mach 0.785, can be approximated using the assumption that a failed wingfan will windmill rather than lock in place. Note that while a good estimate of the drag value is very important for the results of this study, it is the element with the most uncertainty.

Reference 16 states that the drag of a windmilling turbojet engine (as a starting point) can be computed using

$$(D/q) = 0.3A_e \tag{29}$$

$$q = \frac{1}{2} v^2 \rho \tag{30}$$

where A_e is the area of the engine face, the coefficient of drag is 0.3, v is the aircraft speed, and ρ is the air density. At 35,000 ft, Mach 1 is 972.9 ft/sec, so Mach 0.785 = 0.785 · 972.9 ft/sec = 763.7 ft/sec. Air density at 35,000 ft is 7.38×10^{-4} slugs/ft^3 = 7.38×10^{-4} lb·sec^2/ft^4.

Therefore, q = 0.5 · (763.7 ft/sec)^2 · 7.38×10^{-4} lb·sec^2/ft^4 = 215.2 lb/ft^2, so D = 0.3 · A_e · 215.2 lb/ft^2.

Reference 12, which does not account for boost, states that for the contrarotating fans in the underwing configuration, the fan diameter is 2.41 ft, so A_e = 4.56 ft^2.

Therefore, D = 0.3 · 4.56 ft^2 · 215.2 lb/ft^2 = 294.4 lb.

Reference 17 presents two graphical approaches to determine the windmilling drag of a turbojet or turbofan that give wildly different results. One utilizes chart data to determine a theoretical drag coefficient and a subsequent Mach number-based adjustment, both of which are functions of SLS takeoff specific thrust. It then uses Equations (29) and (30) with the new drag coefficient to compute the drag. The charts do not quite go down to a low enough specific thrust value for a wingfan, but by extrapolating, a drag coefficient in the range of 0.01 to 0.02 is obtained. Assuming this extrapolation is reasonable, it conservatively produces a drag value of D = 0.02 · 4.56 ft^2 · 215.2 lb/ft^2 = 19.6 lb. The other methodology uses the product of the air pressure, inlet area, and a graphically determined internal drag value to come up with a drag of about 400±100 lb.

Finally, Reference 18 provides an equation for the drag increment due to a windmilling engine. It incorporates external, or spillage drag, which is proportional to inlet area, and internal drag, which is the change in momentum of the air as it passes through the engine. With some assumptions about temperature and pressure, it provides an equation based on Mach number, inlet and nozzle area, and the ratio of the speed of air in the nozzle exit to the freestream. It also gives representative values of this ratio for different types of engines, including for the bypass portion of a turbofan (0.92). Using this ratio and assuming for simplicity that the fan inlet and nozzle have about the same area, this gives a drag coefficient of 0.23, and a resulting drag of 227 lb.

If the wingfans were to be redesigned to account for boost, they would probably be larger since they would have to produce more thrust at TOC, while the GTF would produce less. This would increase A_e and thus the drag. On the other hand, it should be significantly easier to cause a two-stage fan to windmill than it would a turbojet or turbofan, and a wing redesign that successfully incorporates BLI should reduce drag significantly. On balance, it seems likely that the drag computed using Equations (29) and (30) is overestimated, so for this paper, the drag coefficient in Equation (29) will be reduced from 0.3 to about 0.2, making the drag of the windmilling wingfan about 200 lb at cruise.

For feasibility of the design, a very high-performance power system is required. The electrical components that make up the SUSAN electrical system architecture must have very high specific power and efficiency. Reference 19 provides working assumptions for component efficiencies. For this paper, we assume as above that the efficiency range for each electrical string (generator to wingfan motor) is above 90 percent under normal conditions, with variation due to manufacturing differences.

Figure 7 presents the speed, thrust, and power ranges for the wingfans at the 35,000 ft 0.785 Mach flight condition. These values, shown in Table 1, come from a propulsion system design that does not incorporate boost (Ref. 20). The thrust and power values are similar to the data in Reference 12 (defined at 37,000 ft), which indicates that using a single-stage design that does not include boost, the 16 wingfans produce 7,475 lb of net thrust at TOC, or 467 lb each, using 556.5 kW. For demonstration purposes, we will extend the values in Table 1 at the high end to cover boost.

Reference 20 provides thrust information at several design points. The analysis does not incorporate boost, i.e., the thrust split of approximately 65 percent from the wingfans, 35 percent from the GTF is maintained throughout the climb phase. Still, we can assume for this paper that the thrust requirements will be approximately the same when boost is accounted for, realizing that there will be sizing differences that could slightly change the weight and drag of the aircraft. Table 2 lists the required thrust at the relevant design points. Note that the required TOC wingfan thrust from Reference 12, which again does not account for boost, results in 7,475/0.65 = 11,500 lb total aircraft thrust, which matches the information in Table 2. Although the data in Table 1 and Table 2 represent different altitudes, we will proceed with the assumption that this will not substantially impact the subsequent results.

TABLE 1.—APPROXIMATE RANGES AT THE 35,000 ft 0.785 MACH FLIGHT CONDITION

Variable	Low	High
Speed, rpm	182	403
Net thrust, lb	[a]23	[a]473
Power, kW	44	597

[a] Actual value, curve fit using Equation (25) gives 28 lb at 182 rpm and 470 lb at 403 rpm.

TABLE 2.—SUSAN AIRCRAFT THRUST REQUIREMENTS AT RELEVANT DESIGN POINTS (REF. 20)

Operating Point	Altitude, ft	Mach number	Net thrust, lb
TOC	37,000	0.785	11,500
Cruise	37,000	0.785	7,134

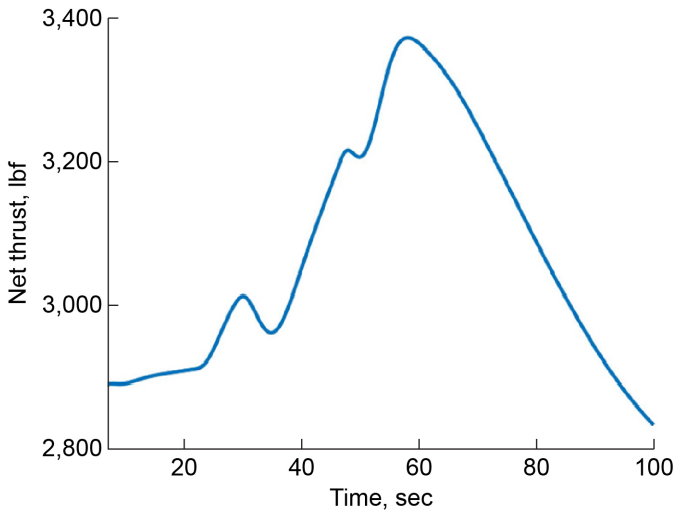

Figure 11.—Temporary thrust increase from GTF during coordinated turn at cruise.

Since the incorporation of boost enables the engine to be sized for cruise, we can assume that the cruise net thrust of 7,134 lb adheres to the 65-35 percent thrust split, while in the boosted region, the GTF thrust would not increase, so the wingfans' share will exceed 65 percent of the total. Currently, boost is envisioned as an augmentation of 2 MW for 5 min at TOC (Ref. 2), which equates to 125 kW per wingfan. Accounting for a worst-case electrical string efficiency of 90 percent, this still leaves 112.5 kW of boost power per wingfan, which corresponds to about 92 lb of additional thrust. Since thrust at TOC is 11,500 lb, maximum normal wingfan thrust is $0.65 \cdot (11{,}500 - 16 \cdot 92) = 6{,}518$ lb which corresponds to about 408 lb per wingfan. Thus, maximum thrust with boost is $408 + 92 = 500$ lb. This is achieved with a wingfan speed of about 411 rpm. A new propulsion system design that accounts for boost would likely produce quite different numbers; these are only used for demonstration purposes.

It is instructive to investigate how the autopilot performs a coordinated turn at cruise to put the final pieces in place. First, during a coordinated turn resulting in a 40° heading change, regardless of whether DEP or the rudder is used, the flight control temporarily increases the GTF thrust by about 16 percent (Figure 11). This means that the nominal wingfan thrust increases by the same proportion. This maximum thrust and corresponding power level must be within the normal range of the powertrain. With DEP, half of the wingfans produce additional thrust, which is balanced by the other half, which produce symmetrically less thrust (Figure 4(b) and Figure 5), approximately maintaining the power level.

Since maximum normal wingfan thrust at the flight condition is about 408 lb and the cruise thrust is $0.65 \cdot 7{,}134/16 = 290$ lb per wingfan, there is quite a large thrust margin available at the upper end. This is designed to accommodate a single wingfan failure (Ref. 20). As can be seen in the wingfan thrust plot of a coordinated turn at cruise shown in Figure 5, there is an asymmetry (compare to Figure 4) caused by a temporary throttle increase to maintain altitude. This throttle increase would not be possible at cruise without the margin. This incursion into the upper normal thrust range is further exacerbated by the differential thrust command. Note that the nominal wingfan speed is related to the throttle setting while the differential thrust commands are added to that. If necessary, it is possible to take advantage of the speed range available for boost to enable the increased thrust on one side, balanced out by a reduction on the other side, to maintain fairly constant power draw from the GTF without battery augmentation.

As stated above, based on the design specifications, the nominal wingfan thrust at cruise should be $0.65 \cdot 7{,}134/16 = 290$ lb. This corresponds to about 372 kW ideally, meaning that the generator must be able to produce $372/0.9 = 413$ kW to account for electrical string efficiency. However, utilizing a dynamic model of the SUSAN vehicle (Ref. 21) and its flight control system (Ref. 22), the aircraft trims at 35,000 ft, Mach 0.785 at a thrust level of about 8,178 lb, meaning that wingfan thrust is about 332 lb, as shown in Figure 5 (the corresponding GTF thrust is shown in the first few seconds of Figure 11). This discrepancy can be partially attributed to the slightly lower altitude, but more likely due to higher weight and drag assumptions in the flight model as compared to the original design. Again, these inconsistencies will be resolved in the final design.

Finally, for this work we assume that wingfans fail abruptly and completely, and that failures are identified instantly to allow for thrust setpoint reallocation.

6.0 Example

For the purposes of this paper, the conflicting information must be reconciled. Having developed the requirements based on the design, the model data shall be scaled to match. Thus, the model data are scaled by $290/332 = 0.8735$ so that the baseline wingfan thrust at cruise is 290 lb. This results in the maximum net thrust accounting for the throttle increase and DEP during the coordinated turn staying within the normal range, i.e., below 408 lb per wingfan. Using the scaled data, the example can proceed with the assumptions listed above.

This control reconfiguration approach is demonstrated here during a coordinated turn. The objective is to fail multiple wingfans and still successfully complete the coordinated turn. The example is shown in Figure 12. Recall that this is thrust setpoint reallocation, there are no actual dynamics shown, rather results that would be achieved with perfect setpoint tracking. Here, the four wingfans connected to a single generator will fail sequentially. Initially, the thrust commands are spread out, i.e., optimized for efficiency as in Figure 8, again using H^8 as the weighting matrix. At 18 sec, the outermost wingfan on the starboard side (no. 17, see Figure 2) fails (Figure 12(a)). Assuming that the failure is identified rapidly, the command to that wingfan is redistributed to the remaining ones, accounting for the drag of the now inoperable wingfan. The thrust of the failed wingfan drops to –200 lb (drag), while on average the commands to the remaining wingfans increase but otherwise retain their general shape initially. At about 25.7 sec, the first wingfan command hits its saturation limit. Because additional thrust is required, several of the remaining wingfan thrust commands increase, while others decrease to maintain the required torque on the aircraft. Over the next few seconds, two more wingfans saturate. By 36 sec, the third wingfan to saturate has unsaturated but the first two wingfans are still saturated when a second failure occurs, this time to the outermost wingfan on the port side (no. 1). Because this wingfan is on the side the aircraft is turning toward, with DEP it is producing relatively little thrust. Thus, while some wingfan thrust commands increase to recover the lost thrust, the two saturated wingfans unsaturate to balance the torque on the aircraft. These two wingfans subsequently resaturate but are both unsaturated by the 49 sec mark. At 50 sec, the innermost wingfan on the starboard side (no. 10) fails, causing an increase in the commands to most of the remaining wingfans, with a noticeable rapid decrease in one and several smaller decreases in others to balance out the torque on the aircraft. As the turn continues, more of the remaining wingfans saturate, especially around the time of the peak in total thrust at about 58 sec (Figure 12(b)). As the thrust decreases, the saturated wingfans unsaturate one by one. At 75 sec, however, the innermost wingfan on the port side (no. 8) fails. This causes an immediate increase in the commands to the remaining wingfans, several of which remain at or near saturation until about 98 sec, when the last saturated wingfan unsaturates. There are always at least two unsaturated wingfans, and all but one of the working wingfans (no. 16) saturate at some point during the turn. Which wingfans saturate has to do with the side of the aircraft they are on (those on the side that the aircraft is turning toward reduce their thrust) and the efficiency of their associated electrical string (less thrust is requested of the least efficient strings). It is interesting to note that using the same scenario but switching the order of the first two failures, no wingfans saturate before the second failure and only two saturate before the third. When all electrical string efficiencies are the same, there are no saturations before the third failure since no particular wingfans are being unduly emphasized (neither of these cases is shown). Success is demonstrated by the fact that both the total commanded thrust (Figure 12(b)) and net torque on the aircraft (Figure 12(c)) match the original unfailed (ideal) values throughout the turn, indicating that the redistribution works as intended and the redundancy within the powertrain is able to accommodate the failure given that there is sufficient power available.

Figure 13 shows the power required from each generator during the coordinated turn. Only the LPS generators are considered in this proof-of-concept example, the small HPS generator is ignored. The colors of the curves correspond to the electrical bus colors in Figure 2. The different initial values indicate the average weighted efficiencies of the electrical strings attached to each generator (this includes the efficiency of the generator itself). The generators with the higher average

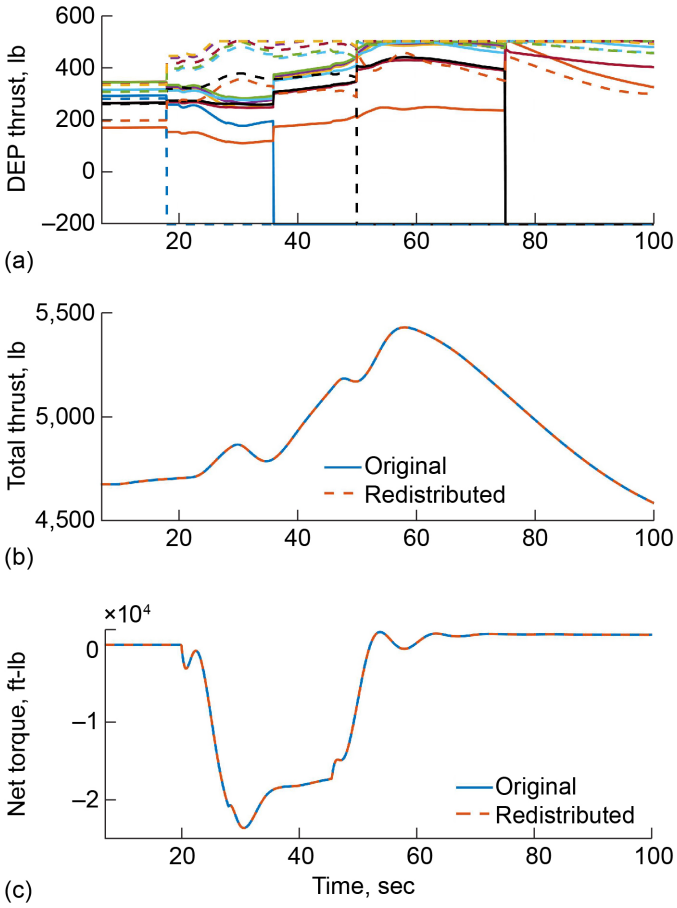

Figure 12.—(a) After scaling the data for the example, redistributed wingfan thrust setpoints, (b) total wingfan thrust for both original unfailed and redistributed commands, and (c) net torque on aircraft for both original unfailed and redistributed commands.

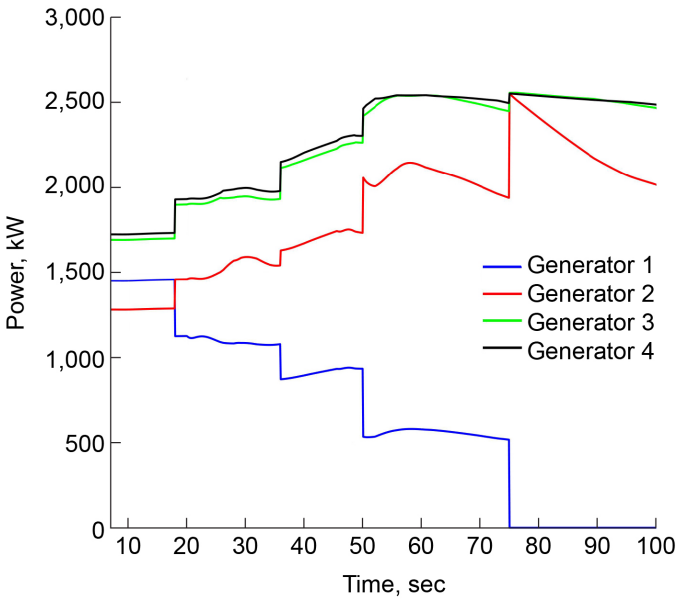

Figure 13.—After scaling the data for the example, power required from each generator during a coordinated turn.

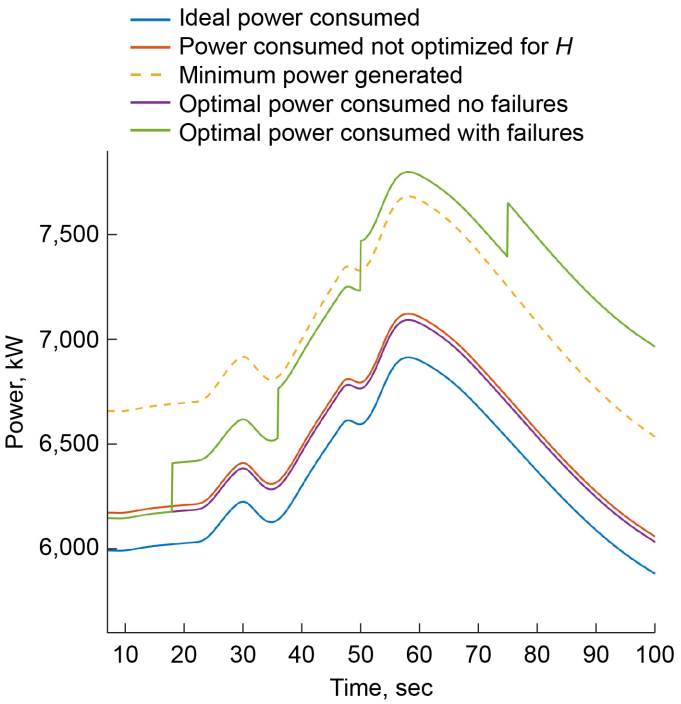

Figure 14.—After scaling the data for the example, total power required during a coordinated turn under various scenarios.

string efficiencies are used more than those with the lower average string efficiencies, so even though the strings are more efficient on average, they require more power. The power demand on Generator 1 (blue line) steps down with each wingfan failure, eventually to zero with the fourth failure, and consequently the power demand on the other generators immediately increases to enable the remaining operational wingfans to provide the necessary thrust. The red line (Generator 2), which corresponds to the least efficient set of electrical strings, starts out lowest. As wingfans fail, it follows the green (Generator 3) and black (Generator 4) curves stepwise but remains consistently below them. However, all along it tracks the general shape of the total thrust curve (Figure 12(b)). After the third failure, Generators 3 and 4 have essentially peaked as their associated wingfans are close to saturation. With the fourth failure, the red line initially jumps up to maintain thrust, but immediately begins to drop off, still mirroring the total thrust curve. We can infer from this behavior that the more efficient wingfans (those associated with Generators 3 and 4) are being used primarily to achieve the required total thrust; the least efficient wingfans (those associated with Generator 2) provide the torque variations on the aircraft (because they are not saturated) while also contributing to total thrust maintenance. It must be noted here that the power lost from Generator 1 is much more than made up for by the increase in power of the three remaining generators because the thrust must now overcome the drag of the inoperable wingfans. Still, no generator approaches its 5 MW limit.

Figure 14 shows several total power requirement scenarios during the coordinated turn. The lowest curve (blue) is the ideal power consumed during a coordinated turn, assuming each electrical string is 100 percent efficient and there are no failures. The red curve (initially the highest solid line) represents the power consumed in the unoptimized case with no failures, where all wingfans are commanded to produce the same initial thrust (before the 20 sec mark in Figure 5), regardless of their electrical string efficiencies. The yellow dashed line indicates the minimum amount of power that must be able to be extracted from the GTF for the unoptimized (red) case, allowing for electrical string efficiencies as low as 90 percent (i.e., blue line divided by 0.9); this does not account for additional power requirements such as battery charging and certainly not emergency power to overcome the drag of a failed wingfan. The red line is much closer to the blue than to the yellow line for the given set of efficiencies because the weighting matrix (H^8) greatly favors the most efficient electrical strings, and recall that the problem was formulated to minimize the square of the power consumption; across-the-board efficiencies of 90 percent would result in the red line overlaying the yellow line. The magenta line denotes the power consumed when the power distribution has been optimized for efficiency, here saving about 0.4 percent when compared to the red curve. Note that the amount of savings depends on the distribution of the electrical string efficiencies (recall that the efficiency of each electrical

string is a random value between 90 and 99 percent), the weighting matrix, and whether the most efficient wingfans saturate. Under the right circumstances, savings of over 1 percent can reasonably be achieved. To put this in perspective, at a cruise condition with 95 percent efficient electrical strings, a 1 percent change in electrical string efficiency results in about a 0.7 percent change in GTF fuel flow, i.e., a 1 percent power savings applied to two-thirds of the thrust[2] (0.67 percent) results in 0.7 percent overall fuel savings. The green line shows the optimized failure scenario. It initially matches the magenta line but jumps up at 18 sec when the first wingfan fails and with each subsequent wingfan failure as the generators react. Here we assume that each inoperative wingfan accounts for 200 lb of drag, so the powertrain must suddenly provide compensating thrust in addition to making up for the lost thrust. The green curve in Figure 14 is the sum of the four curves in Figure 13.

Although, again, the data and numbers used in the example are inconsistent and the quantitative results should not be taken as fact, the general approach and qualitative results are valid. Therefore, the failure scenario described in Figure 14 points out an area of potential concern. Recall that the coordinated turn at cruise must be able to be accomplished within the normal operating range of the powertrain. Here we scaled model data so that the baseline wingfan thrust at cruise matched the design, and subsequently the temporary throttle increase during the coordinated turn remained below the maximum (see Figure 12(b): the total wingfan thrust approaches 5,430 lb, which is well below the 6,518 lb unboosted maximum). We see in this example that matching the total thrust while adhering to the wingfan thrust constraints is easily accomplished but overcoming the drag of potentially even a single failed wingfan may exceed the power extraction capability of the GTF. A more complete implementation of the thrust reallocation that utilizes the HPS power extraction capability could lessen this concern. While there is still thrust and thus power available through an additional throttle increase in this case, the wingfans are thrust/speed limited. This means that although the power extraction can be increased, once the wingfans are saturated, their thrust cannot increase. The implication is that in failure scenarios, the percent of thrust provided by the GTF may need to increase to achieve the desired total thrust, if it is even possible, and matching desired thrust may be at the expense of matching torque on the aircraft used for maneuvering, which in turn can limit the potential size and thus weight reductions of the flight control surfaces. It was stated earlier that the power extraction can vary only a small but unspecified amount at a given flight condition; this variation is necessary to allow for battery charging and differences in electrical string efficiency. The type of fault recovery analysis shown here can help define what that range must be. The drag assumption may be too high as well, but as long as the thrust requirement nears the maximum available, it will take very little additional drag to exceed the limit.

The results of the example were based on multiple assumptions, and were demonstrated at cruise, which may add additional difficulty. For instance, the temporary throttle increase during the coordinated turn is much more significant than for a similar turn at lower altitude. Still, for safety the aircraft must be able to take advantage of the powertrain design's inherent redundancy to maintain operation that is close to normal.

7.0 Conclusion

This paper presented an approach to optimally distribute thrust setpoint commands that accounts for electrical string efficiency, as well as to recover lost wingfan thrust due to failures or saturations. It demonstrated that the ideal thrust and torque on the vehicle can be maintained up to the limits of the powertrain. The problem formulation allows the number and location of fan failures for which the thrust and torque can be maintained to be investigated, which has implications for certification. Although the SUSAN design is not final and many assumptions of uncertain validity were made in this paper, the main finding demonstrated by the example is that the ability to downsize components to save weight, which is enabled by redundancy and benefits of electrification, is somewhat offset by the requirement for safe operation in failure scenarios and graceful degradation. The final design will determine the amount of redundancy that can be leveraged against failures, and how safety requirements will impact the achievable efficiency of the vehicle.

[2]Data from the Numerical Propulsion System Simulation (NPSS) SUSAN cycle design model that uses a two-thirds/one-third rather than 65/35 thrust split and does not incorporate boost.

References

1. Chau, T., Kenway, G., and Kiris, C.C. "Conceptual Exploration of Aircraft Configurations for the SUSAN Electrofan." *AIAA SciTech 2022 Forum*. AIAA 2022-2181. San Diego, CA and online, January 3-7, 2022.
2. Litt, J.S., Kratz, J.L., et al. "Control Architecture for a Concept Aircraft with a Series/Parallel Partial Hybrid Powertrain and Distributed Electric Propulsion." *AIAA SciTech 2023 Forum*. AIAA 2023-1750. National Harbor, MD and online, January 23-27, 2023.
3. Burcham, F.W. Jr., and Gilyard, G.B., "Integrated Flight-Propulsion Control Concepts for Supersonic Transport Airplanes," NASA Technical Memorandum 101728, November 1990.
4. Fuller, J.W., "Integrated Flight and Propulsion Control for Loss-of-Control Prevention," AIAA Guidance, Navigation, and Control Conference, AIAA 2012-4896, Minneapolis, MN, August 13-16, 2012.
5. Tucker, T., "Touchdown: The Development of Propulsion Controlled Aircraft at NASA Dryden," Monographs in Aerospace History #16, 1999.
6. *Restructurable Controls*, NASA Conference Publication 2277, Hampton, VA, September 21-22, 1982.
7. Chau, T., and Duensing, J., "Conceptual Design of the Hybrid-Electric Subsonic Single Aft Engine (SUSAN) Electrofan Transport Aircraft," *AIAA SciTech 2024 Forum*. AIAA 2024-1326. Orlando, FL, January 8-12, 2024.
8. Luenberger, D.G. *Linear and Nonlinear Programming*, Second Edition, Addison-Wesley, Boston (1984).
9. Litt, J.S., Sachs-Wetstone, J.J., Simon, D.L., et al., "Flight Simulator Demonstration and Certification Implications of Powertrain Failure Mitigation in a Partial Turboelectric Aircraft." *AIAA Aviation 2023 Forum*. AIAA 2023-4156. San Diego, CA and Online, June 12-16, 2023.
10. Litt, J.S., Roulette, G. "A Method for Exploiting Redundancy to Accommodate Actuator Limits in Multivariable Systems." NASA TM-106859. 1994.
11. Litt, J.S., Hickman, A., Guo, T.-H. "A New Technique for Compensating Joint Limits in a Robot Manipulator," TM 107330, ARL-TR-1101. October 1996.
12. Byung Joon Lee and May-Fun Liou. "Conceptual Design of Propulsors for the SUSAN Electro-fan Aircraft." *AIAA SCITECH 2022 Forum*. AIAA 2022-2305. San Diego, CA and online, January 3-7, 2022.
13. Jansen, R.H., Kiris, C.C., Chau, T., et al. "Subsonic Single Aft Engine (SUSAN) Transport Aircraft Concept and Trade Space Exploration." *AIAA SciTech 2022 Forum*. AIAA 2022-2179. San Diego, CA and online, January 3-7, 2022.
14. Machado, L., Chau, T., Kenway, G., Duensing, D.C., and Kiris, C.C., "Preliminary Assessment of a Distributed Electric Propulsion System for the SUSAN Electrofan," *AIAA SciTech 2023 Forum*. AIAA 2023-1748. National Harbor, MD and online, January 23-27, 2023.
15. Machado, Leonardo, Chau, Timothy, and Duensing, Jared C., "Toward the Development of an Underwing Boundary Layer Ingesting Distributed Propulsion System for the SUSAN Electrofan," *AIAA SciTech 2024 Forum*. AIAA 2024- 1327. Orlando, FL, January 8-12, 2024.
16. Raymer, D.P. *Aircraft Design: A Conceptual Approach*. AIAA, Reston, VA (1989).
17. Walsh, P.P, and Fletcher, P., *Gas Turbine Performance, Second Edition*, Blackwell Science and ASME Press, Fairfield, NJ (2004).
18. Torenbeek, E., *Synthesis of Subsonic Aircraft Design*, Delft University Press, Delft, The Netherlands (1982).
19. Haglage, J.M., Dever, T.P., Jansen, R.H., Lewis, M.A., "Electrical System Trade Study for SUSAN Electrofan Concept Vehicle", *AIAA SciTech 2022 Forum*. AIAA 2022-2183. San Diego, CA and online, January 3-7, 2022.
20. Chapman, Jeffryes W., Kratz, Jonathan L., Dever, Timothy, et al. "Update on SUSAN Concept Vehicle Power and Propulsion System." *AIAA SciTech 2023 Forum*. AIAA 2023-1749. National Harbor, MD and online, January 23-27, 2023.
21. Sachs-Wetstone, J.J, Litt, J.S., Kratz, J.L., and Buescher, H.E. "SUbsonic Single Aft eNgine (SUSAN) Power/Propulsion System Control Architecture Updates." *AIAA SciTech 2024 Forum*. AIAA-2024-1330. Orlando, FL, January 8-12, 2024.
22. Ogden, N.C., and Patterson, A. "A Framework for Evaluating Distributed Electric Propulsion on the SUSAN Electrofan Aircraft." NASA/TM–20230009523. July 2023.